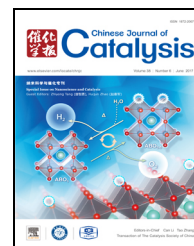


available at www.sciencedirect.comjournal homepage: www.elsevier.com/locate/chnjc

Article (Special Issue on Nanoscience and Catalysis)

Acid-activated and WO_x -loaded montmorillonite catalysts and their catalytic behaviors in glycerol dehydration



Weihua Yu ^{a,b}, Pengpeng Wang ^b, Chunhui Zhou ^{b,c,d,*}, Hanbin Zhao ^b, Dongshen Tong ^b, Hao Zhang ^b, Huimin Yang ^e, Shengfu Ji ^f, Hao Wang ^c

^a Zhijiang College, Zhejiang University of Technology, Hangzhou 310024, Zhejiang, China

^b Research Group for Advanced Materials & Sustainable Catalysis (AMSC), Research Center for Clay Minerals, State Key Laboratory Breeding Base of Green Chemistry Synthesis Technology, Discipline of Industrial Catalysis, College of Chemical Engineering, Zhejiang University of Technology, Hangzhou 310032, Zhejiang, China

^c Centre for Future Materials, University of Southern Queensland, Toowoomba, Queensland 4350, Australia

^d Engineering Research Center of Non-metallic Minerals of Zhejiang Province, Zhejiang Institute of Geology and Mineral Resource, Hangzhou 310007, Zhejiang, China

^e Key Laboratory of High Efficient Processing of Bamboo of Zhejiang Province, China National Bamboo Research Center, Hangzhou 310012, Zhejiang, China

^f State Key Laboratory of Chemical Resource Engineering, Beijing University of Chemical Technology, Beijing 100029, China

ARTICLE INFO

Article history:

Received 13 January 2017

Accepted 10 March 2017

Published 5 June 2017

Keywords:

Glycerol

Acrolein

Dehydration

WO_x

Acid-activated nanoclay

Catalyst

ABSTRACT

The use of H_2SO_4 , HCl , H_3PO_4 , and CH_3COOH -activated montmorillonite (Mt) and WO_x/H_3PO_4 -activated Mt as catalysts for the gas-phase dehydration of glycerol was investigated. The WO_x/H_3PO_4 -activated Mt catalysts were prepared by an impregnation method using H_3PO_4 -activated Mt (Mt-P) as the support. The catalysts were characterized using powder X-ray diffraction, Fourier-transform infrared spectroscopy, N_2 adsorption-desorption, diffuse reflectance ultraviolet-visible spectroscopy, temperature-programmed desorption of NH_3 , and thermogravimetric analysis. The acid activation of Mt and WO_x loaded on Mt-P affected the strength and number of acid sites arising from H^+ exchange, the leaching of octahedral Al^{3+} cations from Mt octahedral sheets, and the types of WO_x ($2.7 \leq x \leq 3$) species (i.e., isolated WO_4/WO_6 -containing clusters, two-dimensional $[WO_6]$ polytungstates, or three-dimensional WO_3 crystals). The strong acid sites were weakened, and the weak and medium acid sites were strengthened when the W loading on Mt-P was 12 wt% (12%W/Mt-P). The 12%W/Mt-P catalyst showed the highest catalytic activity. It gave a glycerol conversion of 89.6% and an acrolein selectivity of 81.8% at 320 °C. Coke deposition on the surface of the catalyst led to deactivation.

© 2017, Dalian Institute of Chemical Physics, Chinese Academy of Sciences.

Published by Elsevier B.V. All rights reserved.

1. Introduction

The use of biodiesel is being developed to address increasing global concerns regarding the environment and sustainable

* Corresponding author. Tel/Fax: +86-571-88320062; E-mail: clay@zjut.edu.cn

The work was supported by the National Natural Science Foundation of China (21373185, 41672033, 21506188, 21404090), the Open Project Programs of Engineering Research Center of Non-metallic Minerals of Zhejiang Province (ZD2015k07), of State Key Laboratory Breeding Base of Green Chemistry-Synthesis Technology (GCTKF2014006), of Key Laboratory of High Efficient Processing of Bamboo of Zhejiang Province (2016), and of State Key Laboratory of Chemical Resource Engineering, Beijing University of Chemical Technology (CRE-2016-C-303).

DOI: 10.1016/S1872-2067(17)62813-4 | <http://www.sciencedirect.com/science/journal/18722067> | Chin. J. Catal., Vol. 38, No. 6, June 2017

development [1–3]. In biodiesel production, a large quantity of glycerol is produced as a by-product [4,5]. Value-added use of glycerol is important in improving the economic viability of the biodiesel industry [6]. One attractive route is the catalytic dehydration of glycerol to the value-added intermediate acrolein [7], which is widely used in the synthesis of pharmaceuticals, detergents, and polymers [8,9]. Acrolein is currently produced by oxidation of propylene, which is derived from non-renewable petroleum, using complex multi-component BiMoO_x-based catalysts [10]. The gas- or liquid-phase dehydration of glycerol using acid catalysts is a more cost-effective and eco-friendly method for acrolein production [3,11].

Acid catalysts such as supported heteropoly acids [12–14], metal oxides [15], zeolites [16,17], and acidic clay minerals [18,19] have been tested in the dehydration of glycerol to produce acrolein. Among these, supported Keggin-type tungstophosphoric acids (H₃PW₁₂O₄₀) on various supports are commonly used for this conversion. Acrolein yields of 75%–86% have been achieved on H₃PW₁₂O₄₀ catalysts using mesoporous silicas such as Cs-SBA-15 [20], W-SBA-15 [6], and HMS [19] as supports. Tsukuda et al. [21] prepared a 30 wt% H₃PW₁₂O₄₀ catalyst (Q6-PW-30) supported on SiO₂ with a mean pore diameter of 6 nm. The catalyst gave an acrolein yield of 64.9% at 325 °C. TiO₂, Al₂O₃, and SiO₂-Al₂O₃ have also been used as supports and gave acrolein yields of 49.6% [22], 51.3% [23], and 19.9% [2], respectively. Yadav et al. [19] reported a 44% acrolein yield using 20 wt% H₃PW₁₂O₄₀ supported on K-10 clay. These catalysts gave inconsistent catalytic performances and were greatly affected by the type of support used. High surface acidities and appropriate pore structures of the catalyst and support are critical factors in achieving high acrolein yields [24]. Although the use of supported H₃PW₁₂O₄₀ catalysts in glycerol dehydration has attracted much attention, their strong acid sites can cause coke formation, and their low thermal stabilities can result in decomposition at the catalyst regeneration temperature (>500 °C), leading to significant decreases in the acidity and activity of the catalyst [20]. Supported H₃PW₁₂O₄₀ catalysts decompose at about 500 °C to P₂O₅ and bulky WO₃, which provide strong Lewis acid sites and are not beneficial for the target acrolein-forming reaction [25]. H₃PW₁₂O₄₀ catalysts are therefore usually prepared by low temperature calcination at 300–400 °C.

WO_x-based materials are promising solid acid catalysts for the gas-phase dehydration of glycerol [26]. Chai et al. [7] prepared a supported WO_x catalyst by impregnation of Al₂O₃ with (NH₄)₆H₂W₁₂O₄₀, followed by calcination at 800 °C. The catalyst consisting of 30 wt% WO₃/Al₂O₃ gave a 61% yield of acrolein in 10 h. Supported WO_x catalysts were similarly prepared by impregnation of ZrO₂, Al₂O₃, and SiO₂ with (NH₄)₁₀W₁₂O₄₁·7H₂O, followed by calcination at 600 °C [14]. The WO_x/ZrO₂, WO_x/Al₂O₃, and WO_x/SiO₂ catalysts gave acrolein yields of 78%, 66%, and 14%, respectively. Supported WO_x catalysts have higher thermal stabilities and stronger acidities than supported H₃PW₁₂O₄₀ catalysts, and they have strong activities in various catalytic reactions [27]. The catalyst acidity depends on the WO_x loading, the preparation method, and the support used.

Montmorillonite (Mt) is a three-layer aluminosilicate clay

composed of a central Al₂O₃ sheet sandwiched between two tetrahedral SiO₂ sheets [28,29]; it has unique attributes such as nanometer-scale platelets, interlayer spaces, a mesoporous structure, and a higher hydrothermal stability than mesoporous SiO₂ supports [30,31]. In addition, Mt can be modified as solid acid catalysts. The Brønsted and Lewis acid sites of Mt can be tailored using surface adsorption [32], ion-exchange reactions [30], pillaring, surface grafting, and impregnation [33,34]. To the best of our knowledge, the present paper is the first report of the use of heat-resistant Mt as a support in the preparation of acid-activated and WO_x-loaded Mt catalysts for glycerol dehydration. The low selectivity for acrolein and catalyst deactivation caused by coking limited large-scale industrial applications of catalytic dehydration of glycerol to acrolein over acid catalysts [3]. The present study furthers our understanding of the effects of the acidic properties on catalyst selectivity and deactivation.

In this work, we prepared the supported WO_x catalysts by acid-activated Mt and impregnation with (NH₄)₁₀W₁₂O₄₁·5H₂O. The catalytic activities of the WO_x-loaded catalysts in the gas-phase dehydration of glycerol were studied using a fixed-bed microreactor. The effects of the WO_x loading, the type of acid used for Mt activation, and the concentration of the glycerol feedstock on glycerol dehydration were investigated.

2. Experimental

2.1. Materials

Ca²⁺-Mt with a cation-exchange capacity of 66 mmol/100 g was obtained from a deposit in Gansu, China. Ammonium paratungstate ((NH₄)₁₀W₁₂O₄₁·5H₂O, analytical grade, WO₃ 85%–90%) was purchased from the Sinopharm Chemical Reagent Co., Ltd., China. H₃PO₄ and CH₃COOH (both analytical grade) were obtained from the Shanghai Lingfeng Chemical Reagent Co., Ltd., China. HCl (analytical grade, 36%–48%) and glycerol were purchased from the Hangzhou Shuanglin Chemical Reagent Co., Ltd., China. H₂SO₄ (analytical grade, 95%–98%) was obtained from the Xilong Chemical Co., Ltd., China. H₂C₂O₄·2H₂O (analytical grade) was obtained from the Shanghai Meixing Chemical Co., Ltd., China. All reagents were used without further purification.

2.2. Catalyst preparation

2.2.1. Preparation of acid-activated Mt

Ca²⁺-Mt was activated with H₂SO₄, HCl, H₃PO₄, or CH₃COOH. In all cases, the Ca²⁺-Mt was first dried at 120 °C for 12 h. The dried Ca²⁺-Mt (5 g) was added to 20 wt% acid solution (20 mL) in a 100-mL beaker. This mixture was heated at 80 °C for 4 h with constant stirring and then cooled to room temperature. The supernatant was discarded and the solid residue, i.e., acid-activated Mt, was washed with deionized water until the pH reached 5–6 and then dried in an air oven at 120 °C for 12 h. The acid-activated Mt samples were denoted by Mt-S, Mt-Cl, Mt-P, and Mt-Ac, for H₂SO₄, HCl, H₃PO₄, and CH₃COOH, respectively.

2.2.2. Preparation of W-impregnated Mt catalysts

W/Mt-P catalysts were prepared by impregnating the Mt-P support (3 g) with an aqueous solution of $(\text{NH}_4)_{10}\text{W}_{12}\text{O}_{41}\cdot 5\text{H}_2\text{O}$ and $\text{H}_2\text{C}_2\text{O}_4\cdot 2\text{H}_2\text{O}$. The W concentrations of the impregnating solutions in the final catalysts were 4, 8, 12, and 16 wt%. The preparation procedure, using the 12 wt% catalyst as an example, was as follows. $(\text{NH}_4)_{10}\text{W}_{12}\text{O}_{41}\cdot 5\text{H}_2\text{O}$ (0.60 g) and $\text{H}_2\text{C}_2\text{O}_4\cdot 2\text{H}_2\text{O}$ (0.12 g) were dissolved in deionized water (6 mL) at 80 °C. Mt-P (3 g) was added to the solution and the resulting mixture was kept static for 10 h at room temperature. After impregnation, the solid product was dried at 12 °C for 12 h, and calcined in a flow of air at 350 °C for 3 h. The samples were labeled as $x\text{W}/\text{Mt-P}$, where x is the weight percentage of W in the final catalyst (i.e., $x = 4\%$, 8% , 12% , and 16%).

2.3. Catalyst characterization

Powder X-ray diffraction (XRD) patterns were obtained using a PANalytical X'Pert PRO diffractometer (40 kV, 40 mA) with Ni-filtered Cu K_α radiation ($\lambda = 0.154$ nm). Fourier-transform infrared (FT-IR) spectra were recorded at room temperature in the region 400–4000 cm^{-1} using a Nicolet 6700 spectrometer at a spectral resolution of 4 cm^{-1} ; the samples were KBr pellets.

N_2 adsorption-desorption isotherms were recorded at -196 °C using a Micromeritics ASAP 2020 instrument. Prior to analysis, the samples were degassed at 300 °C and 1.33×10^{-4} Pa for 12 h. The specific surface areas were calculated from the linear parts of the Brunauer-Emmett-Teller (BET) plots. Pore size distributions were calculated based on the adsorption branches of the N_2 isotherms using the Barret-Joyner-Halenda (BJH) method.

Thermogravimetric (TG) analysis and differential thermogravimetry (DTG) were performed using a Mettler Toledo TGA/DSC 1 instrument. The sample was heated from 30 to 800 °C at a heating rate of 10 °C/min in an air flow at 40 mL/min.

Temperature-programmed desorption of NH_3 (NH_3 -TPD) was used to determine the strengths of the acid sites on the catalyst. The catalyst (100 mg) was degassed up to 300 °C under a N_2 flow for 2 h. The catalyst was cooled to 50 °C, and NH_3 gas was passed over the catalyst for 1 h to adsorb NH_3 on the surface. The physisorbed gas was removed by heating the catalyst to 800 °C at a heating rate of 10 °C/min. The total acidity was determined from the amount of NH_3 desorbed per gram of catalyst.

Diffuse reflectance ultraviolet-visible (DR UV-vis) spectra were performed using a Shimadzu UV-2550 spectrometer in reflection mode with a 10 Å resolution and BaSO_4 as the reference. The spectra were recorded at room temperature in the range 200–800 nm. The Kubelka-Munk function $F(R_\infty)$ was obtained from the DR UV-vis absorbance and the edge energies (E_g) were determined from the linear extrapolation of the straight line of the slope near the absorption edge in the plot of $[F(R_\infty)\cdot h\nu]^{1/\eta}$ versus $h\nu$ based on direct allowed transitions [35], where η is electron transition exponent and $\eta = 1/2$ for direct allowed transitions when monolayer WO_x species covered on the surface of catalysts, and $h\nu$ is the incident photon

energy [36,37].

The amount of free acid in the catalyst was determined using a previously reported titration method [18,38]. The catalyst (0.04 g) was dispersed in aqueous NaOH solution (0.01 mol/L, 20 mL) under stirring for 120 min at room temperature. The resulting slurry was centrifuged and the supernatant was titrated with a standard HCl solution (0.01 mol/L) until the methyl orange indicator turned red. The amount of free acid was calculated as

$$\text{Free acid amount (mmol/g)} = (C_1V_1 - C_2V_2)/m$$

where C_1 and C_2 are the concentrations of the aqueous NaOH and HCl solutions, respectively; V_1 is the volume of the aqueous NaOH solution (20 mL); V_2 is the consumed volume of aqueous HCl solution; and m is the mass of the sample (0.04 g).

2.4. Catalytic reaction and catalyst reuse tests

Catalytic tests were performed in a vertical stainless-steel tubular fixed-bed microreactor of diameter 8.5 mm and height 200 mm. The catalyst (30–40 mesh) was placed in the isothermal region of the reactor and the redundant space in the isothermal region beneath the catalyst bed was filled with quartz and quartz wool. The reaction temperature was monitored using a thermocouple inserted into the middle of the catalyst bed. The catalyst was pretreated at 320 °C for 1 h in a flow of N_2 (10 mL/min). A stream of glycerol aqueous solution (5–20 wt%) was fed into the reactor at a flow rate of 0.1 mL/min using a syringe pump. The reaction products were condensed in a cold trap kept in liquid nitrogen and collected for analysis.

The collected products were dissolved and analyzed using a gas chromatography-mass spectrometry (GC-MS; Shimadzu) system with a capillary column (TC-FFAP, 60 m \times 0.32 mm \times 0.5 μm) and a flame ionization detector. The GC column was operated from 40 to 100 °C with a ramping rate of 10 °C/min for 6 min, and then from 100 to 190 °C with a ramping rate of 20 °C/min, and then kept at 190 °C for 11 min. The results of GC analyses of the liquid phase and gas phase were combined and used to evaluate the conversion, selectivity, and carbon balance. The gaseous by-products and coke deposited on the catalyst were not analyzed quantitatively and their percentages were denoted by "others" to maintain the material balance. The glycerol conversion, product selectivity, and product yield were calculated as:

$$X(\%) = (\text{Moles of glycerol reacted}) / (\text{moles of glycerol fed into the reactor}) \times 100$$

$$S(\%) = (\text{Moles of glycerol converted to a specific product}) / (\text{moles of glycerol reacted}) \times 100$$

$$Y(\%) = X \times S / 100$$

where $X(\%)$ is the glycerol conversion, $S(\%)$ is the selectivity for a specific product in the analyzed sample, and $Y(\%)$ is the yield of a specific product.

Catalyst deactivation was investigated by calcining the used catalyst at 500 °C in air for 4 h in a muffle furnace. The regenerated catalyst was introduced into the reactor for the next run.

3. Results and discussion

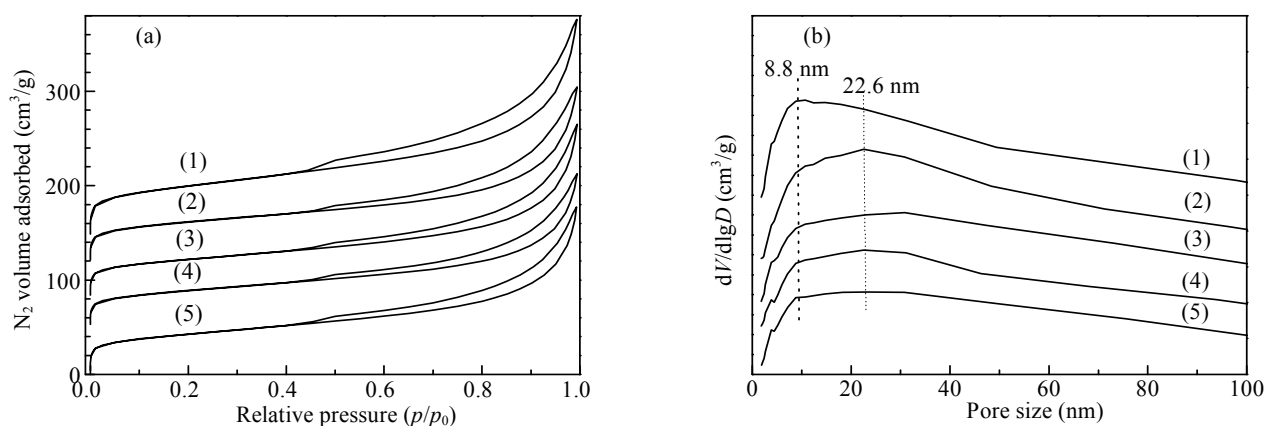


Fig. 1. N₂ adsorption–desorption isotherms (a) and corresponding BJH pore size distributions (b) for Mt-P (1), 4%W/Mt-P (2), 8%W/Mt-P (3), 12%W/Mt-P (4), and 16%W/Mt-P (5).

3.1. Catalyst characterization

3.1.1. Physical properties

The N₂ adsorption–desorption isotherms and BJH pore size distributions of Mt-P and W/Mt-P are shown in Fig. 1. There were no substantial differences between the N₂ adsorption characteristics of the W/Mt-P catalysts and Mt-P, but the BJH pore size distributions were broader. The isotherms of all the catalysts showed type IV profiles and the N₂ adsorption hysteresis loops were H3 type. These adsorption properties suggest that the catalysts consisted of platelet-like particles, which were stacked to form slit-shaped pores [39], and could be considered to correspond to layered structures of Mt-P and W/Mt-P. The stacking of platelet particles resulted in the formation of both micropores and mesopores. The presence of micropores was indicated by the abrupt monolayer adsorption of N₂ at low relative pressures [40]. Filling of the slit-shaped mesopores occurred at higher relative pressures ($P/P_0 > 0.4$) by multilayer adsorption of N₂. Because Mt-P and W/Mt-P showed both microporosity and mesoporosity, the materials had a wide range of pore size distributions, with major pore sizes at 8.8–22.6 nm.

The specific surface areas increased from 97 m²/g for Ca²⁺-Mt to 174 m²/g for Mt-P after activation of Ca²⁺-Mt by H₃PO₄ (Table 1). This increase was caused by partial destruction of the lamellar structure of Mt [41]. Impregnation of Mt-P with WO_x decreased the specific surface area and pore volume

because the WO_x particles were distributed on the external surface of the solid Mt-P and blocked the pore openings [42].

3.1.2. XRD study

The XRD patterns of Ca²⁺-Mt, acid-treated Mt, and the Mt-P-supported WO_x catalysts are shown in Fig. 2. The untreated Ca²⁺-Mt sample showed the typical Mt diffraction peaks from (001), (003), (020), (006), and (060) at $2\theta = 5.89^\circ$, 17.66° , 19.90° , 36.14° , and 62.08° , respectively [43–45]. The d_{001} value was 1.50 nm ($2\theta = 5.89^\circ$), typical of the lamellar structure of Ca²⁺-Mt [46]. Because Mt is a naturally occurring clay mineral, the samples usually contained minor impurities such as feldspar ($2\theta = 22.04^\circ$ and 27.79°) [18,47].

The (001) diffraction peak for acid-activated Mt was stronger and sharper than the corresponding peak for Ca²⁺-Mt; this is in agreement with our previous observations [16]. The results indicate that treatment of Ca²⁺-Mt with 20 wt% acid did not completely destroy the inherent layered structure of Mt. It has been reported that concentrated H₂SO₄ and HNO₃ can cause complete disappearance of the (001) peak for Mt [48–50], and the use of H₃PO₄ broadens and weakens the (001) reflection [45]. The acid strength, acid concentration, and activation time/temperature caused different degrees of destruction of the Mt layered structure [45,50]. Acid treatment also increased the d_{001} value for Mt from 1.50 to 1.56–1.57 nm because of cationic exchange of hydrated Ca²⁺ cations in the interlayer spaces of Mt with H⁺ ions in the aqueous acid solution [51]. Fig. 2

Table 1
Catalyst pore structure data and acidities.

Sample	A_{BET} (m ² /g)	Pore volume (cm ³ /g)	BJH pore size (nm)	W surface density of sample * (W/nm ²)	Total acidity (mmol NH ₃ /g-catalyst)
Ca ²⁺ -Mt	97	0.29	13.6	—	—
Mt-P	174	0.35	8.8	—	2.60
4%W/Mt-P	135	0.28	22.6	1.0	2.83
8%W/Mt-P	127	0.28	22.9	2.1	3.24
12%W/Mt-P	121	0.25	22.6	3.2	3.71
16%W/Mt-P	132	0.27	23.2	4.0	3.35

*W surface density of sample = W loading (wt%) \times $6.02 \times 10^5 / A_{\text{BET}}$ of sample (m²/g)/183.84 (g/mol).

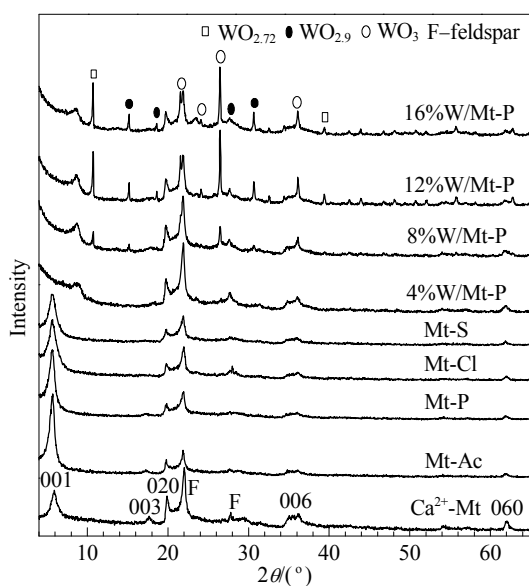


Fig. 2. XRD patterns of Ca^{2+} -Mt, acid-treated Mt, and WO_x -loaded Mt-P.

shows that the intensity of the (001) peak in acid-activated Mt decreased with increasing strength of the acid used, and the (003), (020), (006), and (060) reflections were weakened to different extents or even disappeared after acid activation. These results indicate that the strong acid H_2SO_4 attacked the layered structure most (Mt-S pattern). The strong acids H_2SO_4 and HCl damaged more layers of Mt than did the moderate acid (H_3PO_4) and weak acid (CH_3COOH). The intensities of the feldspar peaks ($2\theta = 22.04^\circ$ and 27.79°) also decreased because of dissolution of this impurity during acid treatment.

For the Mt-P samples impregnated with WO_x , the (001) peak shifted toward higher diffraction angles, indicating a decrease in the interlayer space. This shift is probably caused by the removal of water molecules adsorbed in the Mt interlayer spaces during calcination at 350°C in the preparation of W/Mt-P. The (001) peak of W/Mt-P also became broader and less intense after impregnation with WO_x . This is attributed to the deposition of WO_x nanoparticles on the external surfaces of Mt [42] and/or changes in the pore structure of Mt after impregnation and calcination [52,53].

For W/Mt-P, new peaks appeared at $2\theta = 10.71^\circ$ and 39.42° from $\text{WO}_{2.72}$ [54], at $2\theta = 15.79^\circ$, 18.63° , 19.76° , 27.69° , and 30.66° from $\text{WO}_{2.9}$, and at $2\theta = 21.54^\circ$, 21.90° , 26.45° , and 36.14° from WO_3 [54,55]. The intensities of these WO_x peaks increased with increasing W loading. When the W loading was increased from 12% to 16%, the W surface density increased from 3.2 to 4.0 W/nm^2 (Table 1). A very weak diffraction peak was observed at $2\theta = 23.57^\circ$ – 24.11° , indicating the formation of a stable monoclinic crystalline WO_3 phase (mono- WO_3) [56]. The type of WO_x species present on the supported catalysts depends on the support used. Kim et al. [37] prepared supported WO_3 catalysts by impregnation of Al_2O_3 , Nb_2O_5 , and TiO_2 supports with $(\text{NH}_4)_{10}\text{W}_{12}\text{O}_{41}\cdot 5\text{H}_2\text{O}$. The W surface densities of the Nb_2O_5 and TiO_2 supports were greater than 4.0 W/nm^2 and isolated crystalline WO_3 particles were formed, whereas for the

Al_2O_3 support, no crystalline WO_3 particles were detected. Monotungstate [WO_4] and polytungstate [WO_6] species were both present on the Al_2O_3 -supported WO_x catalyst. In the present work, no monoclinic WO_3 peaks were detected for the 4%W/Mt-P and 8%W/Mt-P samples, probably because of good dispersion of WO_x species on the Mt surface [26].

3.1.3. FT-IR study

FT-IR spectroscopy is an effective tool for probing the chemical and structural properties of Mt. Fig. 3 shows FT-IR spectra of Ca^{2+} -Mt, acid-treated Mt, and the W/Mt-P catalysts. Absorbance bands were observed at 470 cm^{-1} from Si–O bending vibrations, 520 cm^{-1} from Al–O–Si stretching vibrations, and 623 cm^{-1} from the coupling vibrations of Al–O and Si–O. These bands did not change or shift significantly as a result of acid treatment and WO_x impregnation. The presence of the Al–O–Si stretching vibration at 520 cm^{-1} indicates that Mt retained its layered structure [18].

The extent of the changes was assessed based on the intensities of the absorbance bands at 845 cm^{-1} from Mg–OH–Al bending vibrations, 918 cm^{-1} from Al–O–Al bending vibrations, 1039 and 1092 cm^{-1} from Si–O stretching vibrations, 1637 cm^{-1} from H–OH bending vibrations, 3420 cm^{-1} from the stretching vibrations of hydrated water molecules, and 3624 cm^{-1} from the stretching vibrations of hydroxyl groups bonded with octahedral Al^{3+} cations after acid activation [57]. The acid treatment led to the decrease in the intensities of the bands at 845 and 918 cm^{-1} for the acid-activated Mt samples, and the intensities of these bands for Mt-P and Mt-Cl weakened more

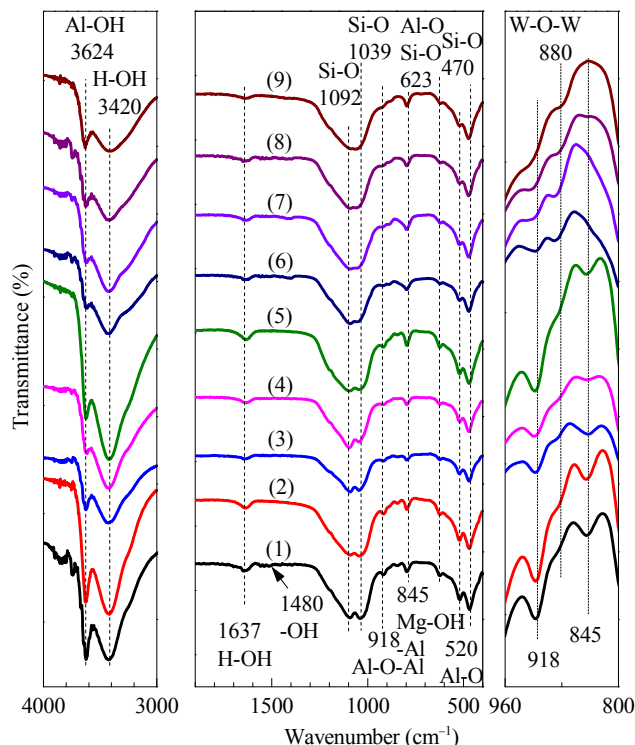


Fig. 3. FT-IR spectra of Ca^{2+} -Mt (1) and the catalysts Mt-Ac (2), Mt-P (3), Mt-Cl (4), Mt-S (5), 4%W/Mt-P (6), 8%W/Mt-P (7), 12%W/Mt-P (8), and 16%W/Mt-P (9).

obviously than for Mt-Ac and Mt-S. The results indicate that more octahedral Al^{3+} cations leached from Mt-Cl and Mt-P than from Mt-S and Mt-Ac [46]. This was confirmed by the decrease in the intensity of the band at 3624 cm^{-1} for Mt-Cl and Mt-P, probably caused by the removal of octahedral Al^{3+} cations as a result of loss of water and the hydroxyl groups coordinated with them [41]. For Mt-Cl, acid treatment significantly increased the intensity of the band at 1092 cm^{-1} . This shows that more Si–O–Si and Al–O–Si bonds were broken and therefore additional Si–OH $_2^+$ and Al–OH $_2^+$ groups were formed on the surface of Mt-Cl [58]. Mt-Cl therefore had a larger number of Brönsted acid sites (Si–OH $_2^+$, Al–OH $_2^+$). A larger number of exposed framework Al^{3+} ions provide more Lewis acid sites [59]. For Mt-S and Mt-Ac, the intensity of this band showed little change. Based on these observations, it is reasonable to conclude that the amount of octahedral Al^{3+} ions released from the Mt lamellar structure during acidification decreased in the order Mt-Cl > Mt-P > Mt-S/Mt-Ac. The larger the number of octahedral Al^{3+} ions that leached from Mt, the more Lewis acid sites became available on the Mt surface [58].

The intensities of the absorption band at 3420 cm^{-1} for the W/Mt-P samples were lower than the intensity of this band for the parent Mt-P. This is because the adsorbed water molecules in the interlayer spaces of Mt were removed during calcination at $350\text{ }^\circ\text{C}$. The additional weak band at 880 cm^{-1} is attributed to the W–O–W vibration mode [60,61]. These results suggest the presence of WO_x in the W/Mt-P samples. These findings are in agreement with the XRD data. For the W/Mt-P samples, the absorption band at 918 cm^{-1} (Al–O–Al) weakened compared with that for Mt-P and the band at 845 cm^{-1} (Mg–OH–Al) disappeared. These results verify the effectiveness of supporting WO_x on Mt-P and the role of Mt-P in creating a coordination microenvironment for these atoms.

3.1.4. TG-DTG analysis

The TG-DTG curves of uncalcined 12%W/Mt-P are shown in Fig. 4. The DTG curve shows three endothermic stages in an air flow. The first endothermic peak, at $61\text{ }^\circ\text{C}$, corresponds to the removal of physically adsorbed water [62]. The second-stage endothermic peaks at 215 , 270 , and $294\text{ }^\circ\text{C}$ represent decomposition of the impregnated precursor $(\text{NH}_4)_{10}\text{W}_{12}\text{O}_{41}\cdot 5\text{H}_2\text{O}$. This stage involves release of crystal water and NH_3 and the

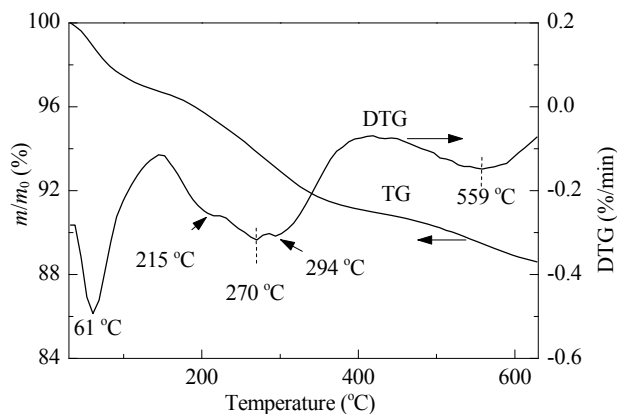
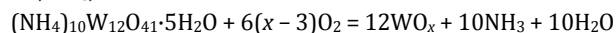


Fig. 4. TG-DTG curves of uncalcined 12%W/Mt-P.

generation of WO_x with various stoichiometric compositions in the temperature range $150\text{--}400\text{ }^\circ\text{C}$ [63,64]. The endothermic peak at $559\text{ }^\circ\text{C}$ is ascribed to removal of the structural hydroxyl groups of Mt [58]. The mass loss for uncalcined 12%W/Mt-P was 11.3% in the temperature range $30\text{--}630\text{ }^\circ\text{C}$ (Table 2), which is equal to the theoretical value (11.2%) for loss of $(\text{NH}_4)_{10}\text{W}_{12}\text{O}_{41}\cdot 5\text{H}_2\text{O}$. In the temperature range between 350 and $500\text{ }^\circ\text{C}$, the mass loss was only 1.4%. This is similar to the mass loss of 1.2% for decomposition of pure $(\text{NH}_4)_{10}\text{W}_{12}\text{O}_{41}\cdot 3.5\text{H}_2\text{O}$ in air in the temperature range $377\text{--}480\text{ }^\circ\text{C}$ [63]. The decomposition of supported $(\text{NH}_4)_{10}\text{W}_{12}\text{O}_{41}\cdot 5\text{H}_2\text{O}$ on the 12%W/Mt-P sample was therefore almost complete at $350\text{ }^\circ\text{C}$. Madarász et al. [65] reported that WO_3 crystallization started from the amorphous state during thermal decomposition of pure $(\text{NH}_4)_{10}\text{W}_{12}\text{O}_{41}\cdot 4\text{H}_2\text{O}$ in calcination between 400 and $500\text{ }^\circ\text{C}$ in air. To avoid agglomeration of WO_x particles and recrystallization of WO_3 caused by calcination at higher temperatures [63,66], in the present work, $350\text{ }^\circ\text{C}$ was used as the calcination temperature for the WO_x -loaded Mt catalysts. The decomposition of $(\text{NH}_4)_{10}\text{W}_{12}\text{O}_{41}\cdot 5\text{H}_2\text{O}$ leads to formation of WO_x , NH_3 , and H_2O :



3.1.5. DR UV-vis spectra study

DR UV-vis spectra can provide information on local structures (isolated, polymeric, clusters, and bulk structures) of covalent-bridged W–O–W bonds on WO_x -loaded catalysts [36]. Fig. 5 shows DR UV-vis spectra of the WO_x -loaded catalysts. All the catalysts showed an absorption band at 256 nm , which is assigned to isolated $[\text{WO}_4]$ tetrahedral species or WO_6 -containing clusters [27,54]. The absorption band shoulder at about $280\text{--}400\text{ nm}$ can be attributed to the presence of octahedral $[\text{WO}_6]$ polytungstate species and crystalline WO_3 [27,36]. The intensity of the absorption shoulder increased with increasing W loading. The appearance of an absorption band for crystalline WO_3 in the spectrum of the 12%–16% W-loaded catalysts confirms the XRD results.

The specific WO_x species in the catalysts were investigated by the E_g values. For 8%W/Mt-P and 12%W/Mt-P, the E_g values were 3.4 and 3.2 eV, respectively; these originate from polytungstate $[\text{WO}_6]$ species. The E_g value for 4%W/Mt-P (3.5 eV) was slightly higher than those for 8%W/Mt-P and 12%W/Mt-P; this is because of the presence of alternating WO_4/WO_6 clusters [36]. The E_g value of 2.8 eV for 16%W/Mt-P corresponds to the characteristic absorption edge energy of

Table 2

Mass losses (%) from catalysts before and after reactions.

Sample	Temperature region ($^\circ\text{C}$)					
	30–150	150–350	350–500	500–630	150–500	150–630
Fresh Mt-P	5.9	0.8	0.9	1.3	1.7	3.0
Used Mt-P	0.6	1.1	3.8	5.0	4.9	9.9
Uncalcined 12%W/Mt-P	3.3	5.0	1.4	1.6	6.4	8.0
Fresh 12%W/Mt-P	4.0	0.8	0.9	1.7	1.7	3.4
Used 12%W/Mt-P	1.3	1.2	2.9	3.5	4.1	7.6

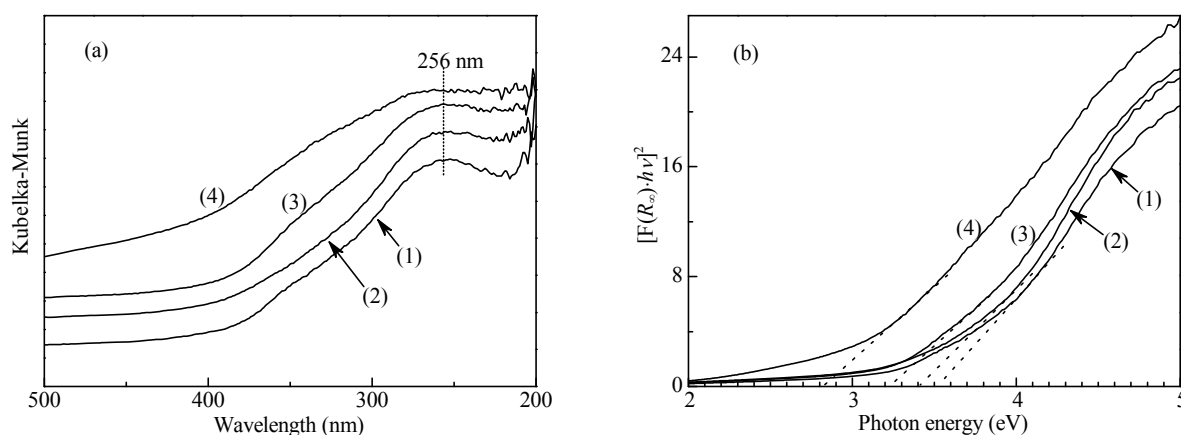


Fig. 5. DR UV-vis spectra of WO_x -loaded catalysts (a) plotted as Kubelka-Munk function vs wavelength and (b) plotted as $[F(R_\infty) \cdot hv]^2$ vs photon energy (1) 4%W/Mt-P; (2) 8%W/Mt-P; (3) 12%W/Mt-P; (4) 16%W/Mt-P.

three-dimensional crystalline WO_3 [67]. These results indicate that dispersed WO_x species formed W–O–W bridging bonds between neighboring WO_x groups to form $[\text{WO}_4/\text{WO}_6]$ -containing clusters, two-dimensional $[\text{WO}_6]$ polytungstates, and isolated three-dimensional WO_3 crystals with increasing W loading from 4% to 16%. WO_x species with different coordination structures provided the WO_x -loaded catalysts with Brønsted and Lewis acid sites.

3.1.6. Generation of acidity on Mt

3.1.6.1. Acid treatment

Raw Ca^{2+} -Mt is a layered aluminum silicate with a 2:1 layered structure predominantly consisting of Al–O octahedral sheets sandwiched by two Si–O tetrahedral sheets. The hydrated Ca^{2+} cations are adsorbed in the interlayer spaces of Mt to balance the negatively charged clay surfaces [29]. Acid treatment can be used to increase the acidity of the raw Ca^{2+} -Mt (Scheme 1). The type of acid used, acid concentration, and reaction conditions (temperature and time) affect the acid sites and the acidity of the acid-activated Mt [45,50,58].

In acid treatment, first, H^+ ions are intercalated into the interlayer spaces of Mt through cation exchange with Ca^{2+} ions. For acid-activated Mt, the acidity is mainly provided by H^+ ions (Brønsted acid sites) hosted by the interlayer spaces of Mt.

When Mt is attacked by an acid, octahedrally coordinated metal ions such as Fe^{3+} and mainly Al^{3+} are preferentially released from the Mt lamellar structure, and the lamellar structure of Mt partially decomposes [50]. Some of the unsaturated Al^{3+} ions (the framework Al sites) are therefore exposed on the external Mt surface. Mt-Cl and Mt-P have the greater numbers of Lewis acid sites than Mt-S and Mt-Ac because of leaching of octahedral Al^{3+} ions from the Mt lamellar structures. These observations are confirmed by the IR spectra. The Lewis acidity of acid-activated Mt generally arises from exposed Al^{3+} ions [59]. Negatively charged Si–O groups are formed by rupture of bonds between Al–O and Si. The negatively charged Si–O groups attract protons, creating Mt Brønsted acid sites.

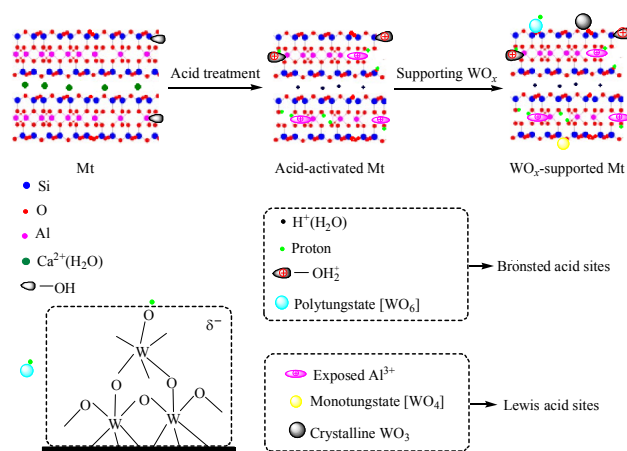
H^+ ions can also be adsorbed by ionized Al–O[−] and Si–O[−]

groups on the external Mt surface. The isoelectric point (pI) of Mt is about 1.47 [68]. In the acidic range ($\text{pH} < \text{pI}$), the Al–OH and Si–OH groups on the Mt surface can take up protons to form Mt- AlOH_2^+ and Mt- SiOH_2^+ . These ions provide Brønsted acid sites on Mt.

The amount of free acid in the acid-activated Mt decreased in the order Mt-P > Mt-Ac > Mt-S > Mt-Cl (Table 3). The free acid arises from H^+ ions adsorbed on the external Mt surface. There is therefore no linear relationship between the amount of free acid and the total acidity.

3.1.6.2. Supported tungsten oxides

The WO_x loading on Mt-P determines the type of Brønsted and Lewis acid sites. The DR UV-vis spectra show that surface monotungstate species (coordinated structure: $[\text{WO}_4/\text{WO}_6]$ clusters), polytungstates (coordinated structure: $[\text{WO}_6]$), and isolated crystalline WO_3 particles were deposited on the surfaces of the WO_x -loaded catalysts (Scheme 1). The polytungstate WO_x species were well dispersed on the catalyst surfaces and provided Brønsted acid sites because the extended network of polytungstate WO_x species had an excess negative charge and could therefore bind protons [69,70]. The mono-



Scheme 1. Generation of acid sites by acid treatment and WO_x loading on Mt.

Table 3Catalytic performances of acid-treated and WO_x-supported Mt catalysts.

Catalyst	Aqueous glycerol (wt%)	Free acid (mmol/g)	X ^a (%)	Y ^b (%)	Selectivity (%)				
					Acrolein	Acetol	Propenol	Acetaldehyde	Others
Mt-Ac	20	1.69	68.2	47.1	69.1	12.3	6.1	4.5	8.0
Mt-P	20	1.73	87.5	63.7	72.8	11.1	5.9	4.8	5.4
Mt-Cl	20	1.58	94.6	59.9	63.3	15.6	9.4	4.7	7.0
Mt-S	20	1.66	65.7	43.1	65.6	13.6	10.2	6.0	4.6
4%W/Mt-P	20	—	65.6	40.9	62.3	13.4	12.0	6.9	5.4
8%W/Mt-P	20	—	69.4	46.7	67.3	13.5	9.2	6.1	3.9
12%W/Mt-P	20	—	93.7	67.3	71.8	10.4	8.6	4.8	4.4
16%W/Mt-P	20	—	75.7	50.7	67.0	11.4	12.2	6.0	3.4
12%W/Mt-P	15	—	89.6	73.3	81.8	6.3	3.9	2.9	5.1
12%W/Mt-P	10	—	76.4	59.8	78.3	6.3	5.7	5.5	4.3
12%W/Mt-P	5	—	72.8	47.2	64.9	10.8	9.7	8.9	5.7

Reaction conditions: catalyst 0.4 g, aqueous glycerol 0.1 mL/min, N₂ carrier gas 10 mL/min, 320 °C, 3 h.^a Conversion of glycerol.^b Yield of acrolein.

tungstate WO_x species and crystalline WO₃ particles provided Lewis acid sites because of the lack of delocalized negative charges for the formation of Brønsted acid sites [71].

In general, the coordinated WO_x structures depend on the WO_x loading (WO_x surface coverage), the preparation process, and the support used [7]. For a support, there is a dispersion threshold for forming monolayer-state WO_x species on the support surface. When the WO_x loading is far lower than the dispersion threshold, WO_x is usually present as monotungstate species. In contrast, when the WO_x loading is close to or over the dispersion threshold, WO_x forms polytungstate species and finally crystalline WO₃ [27].

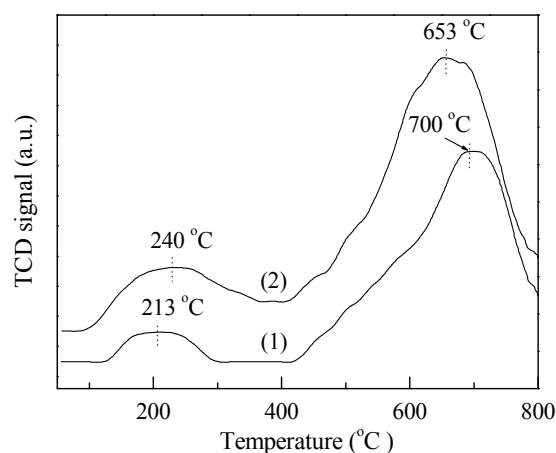
The W surface densities of the catalysts are listed in Table 1. In this work, based on the XRD and DR UV-vis spectra, the dispersion threshold was about 3.2 W/nm² because crystalline WO₃ was detected on 12%W/Mt-P (3.2 W/nm²). 16%W/Mt-P (4.0 W/nm²) provided more Lewis acid sites than 12%W/Mt-P because more mono-WO₃ crystals were formed on the surface of 16%W/Mt-P. For 12%W/Mt-P and 16%W/Mt-P, the loaded WO_x species afforded both Brønsted acid sites and Lewis acid sites. For 4%W/Mt-P (1.0 W/nm²) and 8%W/Mt-P (2.1 W/nm²), which have low surface coverages by WO_x, no mono-WO₃ crystalline particles were detected. The WO_x species on these catalysts therefore provided mainly Lewis acid sites. This is similar to the results reported by Wachs et al. [35]. They loaded WO_x on Al₂O₃, TiO₂, and ZrO₂ supports. Surface monotungstate species (Lewis acid sites) were predominant at low W surface coverages (<2 W/nm²). When the W surface coverage was intermediate, i.e., 3–4 W/nm², surface polytungstate species became predominant and both Brønsted and Lewis acid sites were present. At higher W surface coverages (>4 W/nm²), crystalline WO₃ particles predominated and the number of Lewis acid sites increased.

3.1.7. Acid strength

NH₃-TPD was used to compare the acid strengths of the W-impregnated catalyst and non-impregnated acid-treated Mt-P (Fig. 6). A greater acid strength corresponds to a higher

temperature for desorption of NH₃ adsorbed on acid sites. Acid sites are defined as weak, medium, and strong at desorption temperatures of 50–200, 200–400, and 400–800 °C, respectively [58,72]. Both Mt-P and 12%W/Mt-P showed bimodal acid strengths, reflected by the presence of two desorption stages, at low- and high-temperature regions of about 100–400 and 400–800 °C. Tong et al. [58] suggested that the higher desorption temperature (>400 °C) can be ascribed to desorption of NH₃ adsorbed on framework Al sites (Lewis acid sites). The results suggest that Mt-P and 12%W/Mt-P have acid sites with a broad distribution of acid strengths from weakly to strongly acid.

The acid strength changed after loading WO_x on Mt-P. Low-temperature desorption occurred at 240 °C for 12%W/Mt-P, whereas the corresponding desorption for Mt-P was centered near 213 °C. Loading WO_x on Mt-P shifted the desorption temperature from 213 to 240 °C. These results indicate that the strengths of the overlapped acid sites at 50–200 °C (weak) and 200–400 °C (medium) on 12%W/Mt-P increased. The second desorption occurred at 653 °C for 12%W/Mt-P, whereas the corresponding desorption for Mt-P

**Fig. 6.** NH₃-TPD profiles for Mt-P (1) and 12%W/Mt-P (2).

was centered near 700 °C; this indicates that loading WO_x on Mt-P reduced the strength of the strong acid sites (400–800 °C) in the case of 12%W/Mt-P.

3.2. Catalytic activity

3.2.1. Effect of type of acid used in activation

Mt samples activated by 20 wt% H_2SO_4 , HCl, H_3PO_4 , or CH_3COOH were used as catalysts for the gas phase dehydration of glycerol to acrolein (Table 3). The main reaction product was identified as acrolein. Acetol, acetaldehyde, propenol, and cyclic ethers were also detected. The glycerol conversions showed that the catalytic activities of the acid-activated Mt decreased in the order Mt-Cl > Mt-P > Mt-Ac > Mt-S. The highest glycerol conversion rate, i.e., 94.6%, with an acrolein selectivity of 63.3%, was achieved using Mt-Cl, as a result of its high acidity. The selectivity for acetol achieved with Mt-Cl was also higher than those obtained with Mt-S, Mt-P, and Mt-Ac. This is because Mt-Cl has the largest number of Lewis acid sites. Mt-P gave the highest selectivity for acrolein, i.e., 72.8%, with a maximum acrolein yield of 63.7%. There was no linear relationship between the amount of free acid and glycerol conversion or acrolein selectivity. These findings indicate that the catalytic activity depended on the acidity and acid sites, and free acids did not play a primary role in glycerol conversion or affect the acrolein yield [18].

3.2.2. Effect of W surface density

The W surface density (W/nm^2) on the catalyst affects the catalytic performance in the gas-phase dehydration of glycerol by changing the coordination structures of WO_x species (i.e., the amount and acidity of acid sites) in the catalyst [7,35]. The glycerol conversion depends on the total acidity, and the selectivity for acrolein is related to the presence of Brønsted acid sites [3]. The total acidities of the WO_x -loaded Mt catalysts are listed in Table 1. The amount of acid in the Mt-P sample was 2.60 mmol NH_3/g , which is lower than the reported value (4.30 mmol NH_3/g) for the common clay K-10 Mt [73]. Table 1 shows that when the W surface density increased from 1.0 to 3.2 W/nm^2 , the total acidity increased from 2.83 to 3.71 mmol NH_3/g . When the W surface density was further increased to 4.0 W/nm^2 , the total acidity decreased to 3.35 mmol NH_3/g . The 12%W/Mt-P sample had the highest acidity. The trends in the total acidities of the Mt-P catalysts were similar to those for WO_x -loaded Pd/ Al_2O_3 catalysts prepared using the same precursor, i.e., $(NH_4)_{10}W_{12}O_{41}$, for impregnation [74]. The differences among the total acidities led to large differences among the glycerol conversions.

The glycerol conversions and acrolein selectivities over the WO_x -loaded Mt catalysts increased with increasing W surface density from 1.0 W/nm^2 in 4%W/Mt-P to 3.2 W/nm^2 in 12%W/Mt-P because of the increase in the acidity and the number of Brønsted acid sites; the results depend on appropriate W loadings (Section 3.1.6.2). 12%W/Mt-P gave a maximum glycerol conversion of 93.7%, with an acrolein yield of 67.3%. However, for 16%W/Mt-P, in which the W surface density increased to 4.0 W/nm^2 , the glycerol conversion decreased to

75.7%, with an acrolein yield of 50.7%. The results suggest that the catalytic activity reaches a maximum when the W loading reaches a dispersion threshold. Chai et al. [7] similarly reported that the selectivity for acrolein increased with increasing W surface density up to 4 W/nm^2 , and then declined with further increases in the W surface density up to 16 W/nm^2 for a WO_x -impregnated Al_2O_3 or ZrO_2 catalyst. We also found that the acetol selectivities of the samples with low W loadings, i.e., 4%W/Mt-P (1.0 W/nm^2) and 8%W/Mt-P (2.1 W/nm^2), and that with the highest W loading, i.e., 16%W/Mt-P (4.0 W/nm^2), were higher than that of 12%W/Mt-P (3.2 W/nm^2). This can be attributed to the presence of more Lewis acid sites on the surfaces of 4%W/Mt-P and 8%W/Mt-P because of the presence of monotungstate species, and on 16%W/Mt-P because of crystalline WO_x species [3,7]. In the present work, a 12% W loading was therefore used for the preparation of a catalyst for acrolein production.

It was also found that 4%W/Mt-P and 8%W/Mt-P gave lower glycerol conversions and lower acrolein selectivities than the parent Mt-P. This can be attributed to the following factors: (1) low W loadings on 4%W/Mt-P and 8%W/Mt-P, resulting in more Lewis acid sites; and (2) changes in the textural properties such as decreased surface areas and pore volumes and a broader distribution of pore sizes than in the case of Mt-P (Table 1).

3.2.3. Effect of glycerol feedstock concentration

Feedstocks with various glycerol concentrations (5, 10, 15, and 20 wt%) were used in glycerol dehydration over the 12%W/Mt-P catalyst. It was observed that increasing the glycerol concentration of the aqueous solution from 5 to 20 wt% led to an increase in the glycerol conversion from 72.8% to 93.7%; the acrolein selectivity increased from 64.9% to 81.8%, then decreased to 71.8%, and the acrolein yield increased from 47.2% to 73.3%, and then decreased to 67.3% (Table 3). Acrolein is produced from secondary carbocations and is thermodynamically controlled; acetol, the major by-product, is formed from primary carbocations and is kinetically controlled [2,75]. According to Le Chatelier's principle, water inhibits glycerol dehydration because it is a product of glycerol dehydration. More water shifts the equilibrium and partially suppresses glycerol dehydration [18]. Aqueous glycerol of low concentration (≤ 10 wt%), i.e., containing more water, gives lower glycerol conversions and acrolein yields. However, aqueous glycerol of high concentration can promote hydrogen transfer [76], leading to more cracking and coking. This results in some pore channels becoming inaccessible because of deposition of carbonaceous materials and coverage of some active catalytic active sites with cokes [19,77]. The glycerol conversion and acrolein selectivity obtained using a 20 wt% glycerol solution were therefore lower than those obtained using a 15 wt% glycerol solution. Based on the glycerol conversion rate and acrolein selectivity, 15 wt% aqueous glycerol was therefore used to evaluate the catalyst reusability.

3.3. Deactivation and reuse of catalyst

Catalyst deactivation was studied based on reaction for 1–10 h over fresh and regenerated 12%W/Mt-P catalysts to determine the stability of the catalyst in glycerol dehydration (Fig. 7). For the fresh 12%W/Mt-P catalyst (Fig. 7(a)), glycerol conversion increased from 43.8% to 93.0% with increasing time-on-stream in the first 4 h, and then decreased to 78.1% at 4–6 h. The glycerol conversion remained stable (77.8%–78.1%) at 6–8 h, and then decreased to 66.5% by 10 h. The acrolein selectivity increased from 55.2% to 83.0% in 1 to 2 h and then remained unchanged at 6–8 h. At 8–10 h, the acrolein selectivity decreased slowly to 77.3%. A comparative test was performed using fresh Mt-P to determine the effect of WO_x species on the catalyst stability. Deactivation of the fresh Mt-P catalyst was more serious than that of the fresh 12%W/Mt-P catalyst. After 10 h, the fresh Mt-P catalyst achieved only 55.4% glycerol conversion and 51.0% selectivity for acrolein. The difference between the acid strengths, determined from the NH_3 -TPD data, led to different catalytic performances. Sites that were too strongly acidic accelerated Mt-P deactivation [3]. These results are confirmed by the TG-DTG curves for Mt-P and 12%W/Mt-P before and after the reactions (Fig. 8).

The 12%W/Mt-P catalyst was regenerated by treating the used catalyst in a muffle furnace at 500 °C for 4 h. After 10 h, the regenerated 12%W/Mt-P catalyst gave 53.3% glycerol conversion and 50.8% selectivity for acrolein (Fig. 7(b)). These results show a decrease in the catalytic performance during the reaction period from 2 to 10 h compared with that of the fresh 12%W/Mt-P catalyst.

Catalyst deactivation can be ascribed to coke deposition on the catalyst surface, as shown by TG-DTG analysis (Fig. 8). Two major mass-loss stages were detected in the TG-DTG profiles of the fresh Mt-P and 12%W/Mt-P catalysts. The mass losses at 78 and 605 °C for W/Mt-P and at 63 and 582 °C for 12%W/Mt-P correspond to the release of physically adsorbed water molecules and dehydration of the Mt structure, respectively [62]. This indicates that no organic matter was present on the fresh Mt-P and 12%W/Mt-P catalysts. After their use in the reactions, rapid mass loss in the temperature region 150–630 °C was observed in the TG-DTG curves of the Mt-P

and 12%W/Mt-P catalysts. This mass loss was caused by the removal of organic species on the catalysts. The amounts of organic species deposited on the Mt-P and 12%W/Mt-P catalysts are listed in Table 2. The mass losses in the temperature region 150–350 °C were about 1.1% and 1.2% for the used Mt-P and 12%W/Mt-P catalysts, respectively, whereas in the temperature regions 350–500 and 500–630 °C, the mass losses were 3.8% and 5.0%, respectively, for the used Mt-P, i.e., higher than those of 2.9% and 3.5%, respectively, for the used 12%W/Mt-P. The total mass loss for the used Mt-P catalyst (9.9%) was higher than that for the used 12%W/Mt-P catalyst (7.6%) in the temperature region 150–630 °C. Dalil et al. [77] studied carbon deposition during gas-phase glycerol dehydration over a WO_3/TiO_2 catalyst. TG analysis at 500 °C showed that the mass loss of the coked WO_3/TiO_2 catalyst was 4.6% (the mass fraction of carbon); this is higher than that of the used 12%W/Mt-P catalyst (4.1% at 500 °C) and lower than that of the used Mt-P (4.9% at 500 °C) in the present work. The results suggest that deactivation of the Mt-P catalyst is easier than 12%W/Mt-P catalyst deactivation because the strong acid sites of Mt-P are stronger than those of 12%W/Mt-P, as shown by the NH_3 -TPD data. The catalyst stability was therefore related to the strength of the strong acid sites.

3.4. Reaction mechanism

Reaction mechanisms for gas-phase dehydration of glycerol over different types of acidic and basic catalysts have been proposed by several research groups [3,19]. The reaction pathways shown in Scheme 2 are postulated based on the reaction mechanism proposed by Tsukuda et al. [21] and the catalytic performances of the acid-activated and WO_x -loaded catalysts in the present work. A proton from a Brønsted acid site attacks the secondary hydroxyl group of glycerol to form the unstable intermediate 1,3-dihydroxypropene, which tautomerizes to 3-hydroxypropanal. 3-Hydroxypropanal is unstable and is dehydrated to acrolein via a keto-enol rearrangement. The unstable 3-hydroxypropanal can also decompose to formaldehyde and acetaldehyde. The formaldehyde reacts continuously with glycerol to form other by-products such as 1,3-dioxan-5-ol

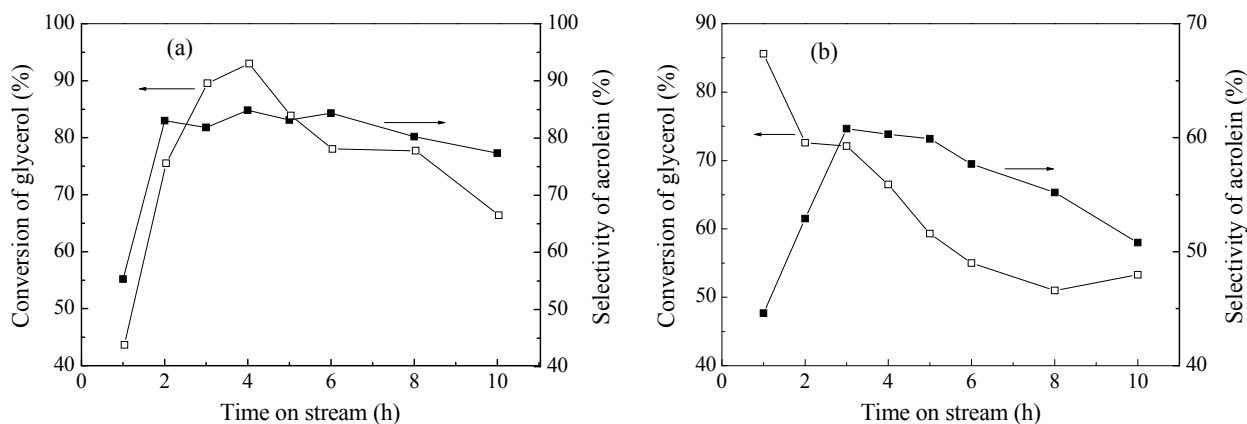


Fig. 7. Deactivation and reuse of 12%W/Mt-P. (a) Fresh catalyst; (b) regenerated catalyst. Reaction conditions: glycerol concentration 15 wt%, aqueous glycerol 0.1 mL/min, N_2 carrier gas 10 mL/min, 320 °C.

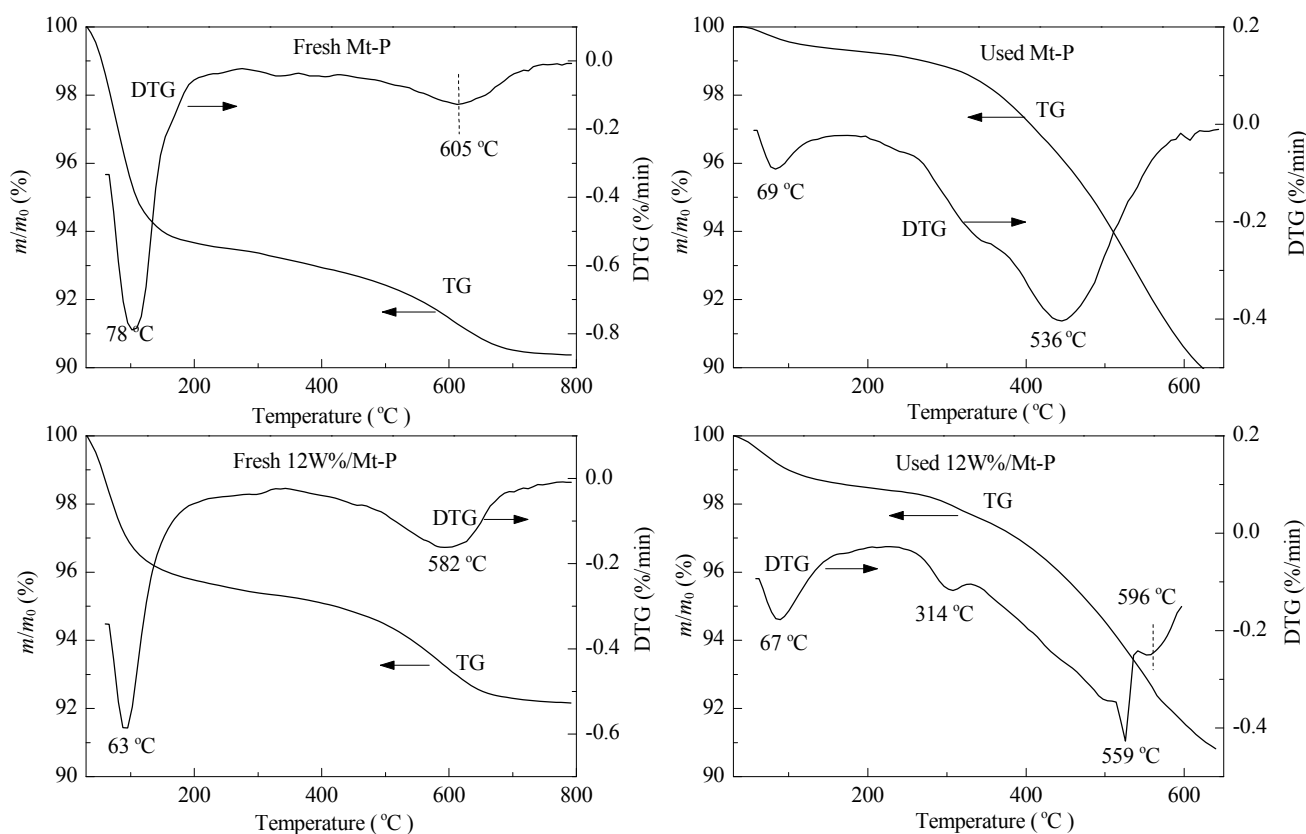
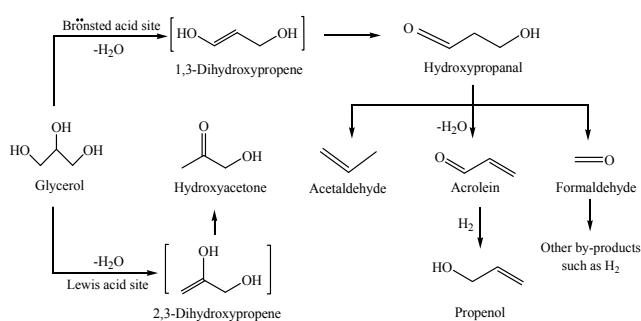


Fig. 8. TG-DTG curves of Mt-P and 12%W/Mt-P before and after reactions.



Scheme 2. Reaction pathways in catalytic dehydration of glycerol over acid catalysts.

and hydrogen [78]; therefore formaldehyde is not detected in the products. The formed hydrogen reacts with acrolein to form propenol [79]. Protonation of a terminal hydroxyl group of glycerol at a Lewis acid site results in formation of the unstable intermediate 2,3-dihydroxypropene, which tautomerizes to acetol.

4. Conclusions

Acid treatment of Mt with 20 wt% H_2SO_4 , HCl, H_3PO_4 , or CH_3COOH at 80 °C for 4 h did not substantially alter the layered structure of Mt. Such acid activation removed some of the impurities in the raw Mt clay and converted Ca^{2+} -Mt to H^+ -Mt by ion exchange. It also led to leaching of some octahedral Al^{3+} ions from the Mt lamellar structure and an increase in the spe-

cific surface area from 97 m^2/g for raw Ca^{2+} -Mt to 174 m^2/g for Mt-P.

WO_x -loaded Mt-P catalysts were prepared by impregnation of Mt-P with 4–16 wt% W. The W loading affected the type of WO_x species on the catalyst surface. The addition of 12% W to Mt-P gave suitable acid sites and appropriate acid strengths for achieving higher catalytic activity and better resistance to deactivation compared with the parent Mt-P and other W/Mt-P catalysts. The highest acrolein yield, i.e., 73.3%, and a glycerol conversion of 89.6% were achieved at 320 °C using an aqueous 15 wt% glycerol solution as the feedstock. When more than 12% W was loaded on the Mt-P, a monoclinic crystalline WO_3 phase was formed.

The catalytic performance of the catalysts was affected by the type of acid used in the activation, the surface coverage by W, and the glycerol concentration in the feedstock. Mt treated with H_3PO_4 (Mt-P) was highly selective for acrolein in gas-phase dehydration of glycerol. A W/Mt-P catalyst with a W surface coverage of 3.2 W/nm^2 and a feedstock concentration of 15 wt% glycerol was the best choice for glycerol dehydration to acrolein.

The catalyst suffered from deactivation and the regenerated catalyst showed decreased activity. The strength of the acid sites was responsible for the catalyst stability. High-strength strong acid sites resulted in easy deactivation of Mt-P. Further investigations are needed to better understand glycerol dehydration and improve the stability and dispersion of WO_x species in WO_x -loaded Mt catalysts.

References

- [1] A. B. F. Moreira, A. M. Bruno, M. M. V. M. Souza, R. L. Manfro, *Fuel Process. Technol.*, **2016**, 144, 170–180.
- [2] T. H. Kang, J. H. Choi, Y. Bang, J. Yoo, J. H. Song, W. Joe, J. S. Choi, I. K. Song, *J. Mol. Catal. A*, **2015**, 396, 282–289.
- [3] B. Katryniok, S. Paul, V. Bellière-Baca, P. Rey, F. Dumeignil, *Green Chem.*, **2010**, 12, 2079–2098.
- [4] A. Seretis, P. Tsiakaras, *Fuel Process. Technol.*, **2016**, 142, 135–146.
- [5] Z. Q. Wang, Z. Zhang, W. J. Yu, L. D. Li, M. H. Zhang, Z. B. Zhang, *Fuel Process. Technol.*, **2016**, 142, 228–234.
- [6] E. Krалева, R. Palcheva, L. Dimitrov, U. Armbruster, A. Bruckner, A. Spojakina, *J. Mater. Sci.*, **2011**, 46, 7160–7168.
- [7] S. H. Chai, B. Yan, L. Z. Tao, Y. Liang, B. Q. Xu, *Catal. Today*, **2014**, 234, 215–222.
- [8] C. H. Zhou, H. Zhao, D. S. Tong, L. M. Wu, W. H. Yu, *Catal. Rev. Sci. Eng.*, **2013**, 55, 369–453.
- [9] G. Paulo da Silva, M. Mack, J. Contiero, *Biotechnol. Adv.*, **2009**, 27, 30–39.
- [10] A. Talebian-Kiakalaieh, N. A. S. Amin, H. Hezaveh, *Renew. Sust. Energy Rev.*, **2014**, 40, 28–59.
- [11] L. Q. Shen, H. B. Yin, A. L. Wang, X. F. Lu, C. H. Zhang, F. Chen, Y. T. Wang, H. J. Chen, *J. Ind. Eng. Chem.*, **2014**, 20, 759–766.
- [12] L. Q. Shen, H. B. Yin, A. L. Wang, Y. H. Feng, Y. T. Shen, Z. A. Wu, T. S. Jiang, *Chem. Eng. J.*, **2012**, 180, 277–283.
- [13] A. Martin, U. Armbruster, H. Atia, *Eur. J. Lipid Sci. Technol.*, **2012**, 114, 10–23.
- [14] M. Massa, A. Andersson, E. Finocchio, G. Busca, F. Lenrick, L. R. Wallenberg, *J. Catal.*, **2013**, 297, 93–109.
- [15] P. Lauriol-Garbry, G. Postole, S. Loridant, A. Auroux, V. Belliere-Baca, P. Rey, J. M. M. Millet, *Appl. Catal. B*, **2011**, 106, 94–102.
- [16] B. Katryniok, S. Paul, F. Dumeignil, *ACS Catal.*, **2013**, 3, 1819–1834.
- [17] H. P. Decolatti, B. O. Dalla Costa, C. A. Querini, *Microporous Mesoporous Mater.*, **2015**, 204, 180–189.
- [18] H. Zhao, C. H. Zhou, L. M. Wu, J. Y. Lou, N. Li, H. M. Yang, D. S. Tong, W. H. Yu, *Appl. Clay Sci.*, **2013**, 74, 154–162.
- [19] G. D. Yadav, R. V. Sharma, S. O. Katole, *Ind. Eng. Chem. Res.*, **2013**, 52, 10133–10144.
- [20] R. Liu, T. F. Wang, Y. Jin, *Catal Today*, **2014**, 233, 127–132.
- [21] E. Tsukuda, S. Sato, T. Takahashi, T. Sodesawa, *Catal. Commun.*, **2007**, 8, 1349–1353.
- [22] L. Q. Shen, Y. H. Feng, H. B. Yin, A. L. Wang, L. B. Yu, T. S. Jiang, Y. T. Shen, Z. A. Wu, *J. Ind. Eng. Chem.*, **2011**, 17, 484–492.
- [23] H. Atia, U. Armbruster, A. Martin, *J. Catal.*, **2008**, 258, 71–82.
- [24] B. Katryniok, S. Paul, M. Capron, F. Dumeignil, *ChemSusChem.*, **2009**, 2, 719–730.
- [25] S. H. Chai, H. P. Wang, Y. Liang, B. Q. Xu, *Green Chem.*, **2008**, 10, 1087–1093.
- [26] M. Massa, A. Andersson, E. Finocchio, G. Busca, *J. Catal.*, **2013**, 307, 170–184.
- [27] K. S. Song, H. B. Zhang, Y. H. Zhang, Y. Tang, K. J. Tang, *J. Catal.*, **2013**, 299, 119–128.
- [28] L. M. Wu, D. S. Tong, C. S. Li, S. F. Ji, C. X. Lin, H. M. Yang, Z. K. Zhong, C. Y. Xu, W. H. Yu, C. H. Zhou, *Appl. Clay Sci.*, **2016**, 119, 116–125.
- [29] C. H. Zhou, J. Keeling, *Appl. Clay Sci.*, **2013**, 74, 3–9.
- [30] B. Thomas, V. G. Ramu, S. Gopinath, J. George, M. Kurian, G. Laurent, G. L. Drisko, S. Sugunan, *Appl. Clay Sci.*, **2011**, 53, 227–235.
- [31] C. H. Zhou, X. Xia, C. X. Lin, D. S. Tong, J. Beltramini, *Chem. Soc. Rev.*, **2011**, 40, 5588–5617.
- [32] T. Santhi, S. Manonmani, T. Smitha, *J. Hazard. Mater.*, **2010**, 179, 178–186.
- [33] P. C. Joshi, M. F. Aldersley, J. W. Delano, J. P. Ferris, *J. Am. Chem. Soc.*, **2009**, 131, 13369–13374.
- [34] C. H. Zhou, *Appl. Clay Sci.*, **2011**, 53, 97–105.
- [35] I. E. Wachs, T. Kim, E. I. Ross, *Catal. Today*, **2006**, 116, 162–168.
- [36] E. I. Ross-Medgaarden, I. E. Wachs, *J. Phys. Chem. C*, **2007**, 111, 15089–15099.
- [37] T. Kim, A. Burrows, C. J. Kiely, I. E. Wachs, *J. Catal.*, **2007**, 246, 370–381.
- [38] S. K. Bharadwaj, P. K. Boruah, P. K. Gogoi, *Catal. Commun.*, **2014**, 57, 124–128.
- [39] M. Kruk, M. Jaroniec, *Chem. Mater.*, **2001**, 13, 3169–3183.
- [40] P. Kumar, R. V. Jasra, T. S. G. Bhat, *Ind. Eng. Chem. Res.*, **1995**, 34, 1440–1448.
- [41] T. H. Wang, T. Y. Liu, D. C. Wu, M. H. Li, J. R. Chen, S. P. Teng, *J. Hazard. Mater.*, **2010**, 173, 335–342.
- [42] J. P. Kumar, P. V. R. K. Ramacharyulu, G. K. Prasad, B. Singh, *Appl. Clay Sci.*, **2015**, 116, 263–272.
- [43] W. H. Yu, Q. Q. Ren, D. S. Tong, C. H. Zhou, H. Wang, *Appl. Clay Sci.*, **2014**, 97–98, 222–234.
- [44] L. Le Forestier, F. Muller, F. Villieras, M. Pelletier, *Appl. Clay Sci.*, **2010**, 48, 18–25.
- [45] L. Zatta, L. P. Ramos, F. Wypych, *Appl. Clay Sci.*, **2013**, 80–81, 236–244.
- [46] L. M. Wu, D. S. Tong, L. Z. Zhao, W. H. Yu, C. H. Zhou, H. Wang, *Appl. Clay Sci.*, **2014**, 95, 74–82.
- [47] Z. Mojović, P. Banković, A. Milutinović-Nikolić, B. Nedić, D. Jovanović, *Appl. Clay Sci.*, **2010**, 48, 179–184.
- [48] D. S. Tong, X. Xia, X. P. Luo, L. M. Wu, C. X. Lin, W. H. Yu, C. H. Zhou, Z. K. Zhong, *Appl. Clay Sci.*, **2012**, 74, 147–153.
- [49] N. Yildiz, Z. Aktas, A. Calimli, *Particulate Sci. Technol.*, **2004**, 22, 21–33.
- [50] Y. H. Zhao, Y. J. Wang, Q. Q. Hao, Z. T. Liu, Z. W. Liu, *Fuel Process. Technol.*, **2015**, 136, 87–95.
- [51] D. Olszewska, *Appl. Clay Sci.*, **2011**, 53, 353–358.
- [52] K. V. Bineesh, M. Kim, G. H. Lee, M. Selvaraj, D. W. Park, *Appl. Clay Sci.*, **2013**, 74, 127–134.
- [53] T. T. Li, J. F. Zhang, X. M. Xie, X. M. Yin, X. An, *Fuel*, **2015**, 143, 55–62.
- [54] H. Liu, K. Tao, H. B. Yu, C. Zhou, Z. Ma, D. S. Mao, S. H. Zhou, *Comptes Rendus Chimie*, **2015**, 18, 644–653.
- [55] I. M. Szilágyi, J. Madarász, G. Pokol, P. Király, G. Tárkányi, S. Saukko, J. Mizsei, A. L. Tóth, A. Szabó, K. Varga-Josepovits, *Chem. Mater.*, **2008**, 20, 4116–4125.
- [56] F. Corà, A. Patel, N. M. Harrison, R. Dovesi, C. R. A. Catlow, *J. Am. Chem. Soc.*, **1996**, 118, 12174–12182.
- [57] M. A. Vicente-Rodriguez, M. Suarez, M. A. Banares-Munoz, J. D. Lopez-Gonzalez, *Spectrochim. Acta Part A*, **1996**, 52, 1685–1694.
- [58] D. S. Tong, Y. M. Zheng, W. H. Yu, L. M. Wu, C. H. Chun, *Appl. Clay Sci.*, **2014**, 100, 123–128.
- [59] M. K. Yadav, C. D. Chudasama, R. V. Jasra, *J. Mol. Catal.*, **2004**, 216, 51–59.
- [60] J. Díaz-Reyes, R. J. Delgado-Macuil, V. Dorantes-García, A. Pérez-Benítez, J. A. Balderas-López, J. A. Ariza-Ortega, *Mater. Sci. Eng. B*, **2010**, 174, 182–186.
- [61] G. S. Rao, N. P. Rajan, M. H. Sekhar, S. Ammaji, K. V. R. Chary, *J. Mol. Catal. A*, **2014**, 395, 486–493.
- [62] H. M. Liu, P. Yuan, Z. H. Qin, D. Liu, D. Y. Tan, J. X. Zhu, H. P. He, *Appl. Clay Sci.*, **2013**, 80, 398–406.
- [63] M. J. G. Fait, H. J. Lunk, M. Feist, M. Schneider, J. N. Dann, T. A. Frisk, *Thermochim. Acta*, **2008**, 469, 12–22.
- [64] A. M. Baghdasaryan, O. M. Niazyan, H. L. Khachatryan, S. L.

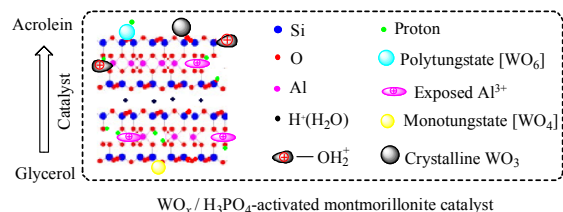
Graphical Abstract

Chin. J. Catal., 2017, 38: 1087–1100 doi: 10.1016/S1872-2067(17)62813-4

Acid-activated and WO_x-loaded montmorillonite catalysts and their catalytic behaviors in glycerol dehydration

Weihua Yu, Pengpeng Wang, Chunhui Zhou*, Hanbin Zhao, Dongshen Tong, Hao Zhang, Huimin Yang, Shengfu Ji, Hao Wang
 Zhejiang University of Technology, China; University of Southern Queensland, Australia; Zhejiang Institute of Geology and Mineral Resource, China; China National Bamboo Research Center, China; Beijing University of Chemical Technology, China

Catalysts consisting of WO_x supported on H₃PO₄-activated montmorillonite showed high activities in glycerol conversion to acrolein. The WO_x state was related to the acid type, strength, and amount on the support surface.



- Kharatyan, *Int. J. Refract. Metal Hard Mater.*, **2014**, 43, 216–221.
- [65] J. Madarász, I. M. Szilágyi, F. Hange, G. Pokol, *J. Anal. Appl. Pyrolysis*, **2004**, 72, 197–201.
- [66] M. Ardestani, H. Arabi, H. R. Rezaie, H. Razavizadeh, *Int. J. Refract. Metal Hard Mater.*, **2009**, 27, 796–800.
- [67] D. G. Barton, M. Shtein, R. D. Wilson, S. L. Soled, E. Iglesia, *J. Phys. Chem. B*, **1999**, 103, 630–640.
- [68] W. H. Yu, N. Li, D. S. Tong, C. H. Zhou, C. X. Lin, C. Y. Xu, *Appl. Clay Sci.*, **2013**, 80–81, 443–452.
- [69] D. G. Barton, S. L. Soled, G. D. Meitzner, G. A. Fuentes, E. Iglesia, *J. Catal.*, **1999**, 181, 57–72.
- [70] C. D. Baertsch, S. L. Soled, E. Iglesia, *J. Phys. Chem. B*, **2001**, 105, 1320–1330.
- [71] S. García-Fernández, I. Gandarias, J. Requies, M. B. Güemez, S. Bennici, A. Auroux, P. L. Arias, *J. Catal.*, **2015**, 323, 65–75.
- [72] D. Liu, P. Yuan, H. M. Liu, D. Y. Tan, H. P. He, J. X. Zhu, T. H. Chen, *Appl. Clay Sci.*, **2013**, 80, 407–412.
- [73] G. B. B. Varadwaj, S. Rana, K. Parida, *Chem. Eng. J.*, **2013**, 215–216, 849–858.
- [74] S. H. Zhu, X. Q. Gao, Y. L. Zhu, Y. W. Li, *J. Mol. Catal. A*, **2015**, 398, 391–398.
- [75] C. J. Yue, M. M. Gan, L. P. Gu, Y. F. Zhuang, *J. Taiwan Inst. Chem. Eng.*, **2014**, 45, 1443–1448.
- [76] C. S. Carriço, F. T. Cruz, M. B. Santos, H. O. Pastore, H. M. C. Andrade, A. J. S. Mascarenhas, *Microporous Mesoporous Mater.*, **2013**, 181, 74–82.
- [77] M. Dalil, D. Carnevali, J. L. Dubois, G. S. Patience, *Chem. Eng. J.*, **2015**, 270, 557–563.
- [78] J. Deleplanque, J. L. Dubois, J. F. Devaux, W. Ueda, *Catal. Today*, **2010**, 157, 351–358.
- [79] S. H. Chai, H. P. Wang, Y. Liang, B. Q. Xu, *Green Chem.*, **2007**, 9, 1130–1136.

催化甘油脱水反应的酸活化蒙脱石负载WO_x催化剂的研究俞卫华^{a,b}, 王朋朋^b, 周春晖^{b,c,d,*}, 赵汉彬^b, 童东绅^b, 张浩^b, 杨慧敏^e, 季生福^f, 王浩^c^a浙江工业大学之江学院, 浙江杭州310024, 中国^b浙江工业大学化学工程学院, 绿色化学合成技术国家重点实验室培育基地, 浙江杭州310032, 中国^c南昆士兰大学未来材料研究所, 图文巴4350, 澳大利亚^d浙江省地质矿产研究所, 浙江省非金属矿物工程研究中心, 浙江杭州310007, 中国^e国家林业局竹子研究开发中心, 浙江省竹子高效加工重点实验室, 浙江杭州310012, 中国^f北京化工大学, 化工资源有效利用国家重点实验室, 北京100029, 中国

摘要: 甘油是一种可由生物资源生产、可持续的、可降解的平台化学品, 是生物柴油、肥皂化工等工业生产过程中的主要副产物。催化甘油脱水反应生产丙烯醛, 有望能替代丙烯等石油裂解产物合成丙烯醛的传统工业路线。丙烯醛是一种重要的化工中间体, 被用于合成蛋氨酸、丙烯酸、3-甲基吡啶和1,3-丙二醇, 并被广泛地应用于农药、医药、高分子材料等领域。随着全球可持续能源发展, 生物柴油生产迅速发展, 将产生大量的副产物甘油。利用甘油为原料, 通过合适的催化剂的催化脱水反应生成丙烯醛, 是近十多年来国内外工业催化的研究热点之一。

用于催化甘油脱水合成丙烯醛的酸催化剂有杂多酸、金属氧化物、沸石与酸性粘土矿物等。钨磷杂多酸(H₃PW₁₂O₄₀)负载的催化剂虽然具有较强的酸性, 有利于催化甘油脱水, 但容易导致结焦, 而且热稳定差, 容易失活。钨磷杂多酸负载于SiO₂, TiO₂, Al₂O₃, SiO₂-Al₂O₃, K-10蒙脱石上表现出不同的催化活性, 表明催化剂和载体的表面酸性和孔结构影响催化性能。近来研究发现, 负载于ZrO₂, Al₂O₃的钨氧化物(WO_x)催化剂热稳定性好、酸性高, 在甘油脱水反应生成丙烯醛中表现出良好的催化性能。但有关钨氧化物(WO_x)结构、催化活性受载体组成、酸性影响的本质和规律一直不清楚。本文采用20 wt%的硫酸、盐酸、磷酸和乙酸对蒙脱石进行酸改性, 并在磷酸改性的蒙脱石上负载W含量为4–16 wt%的WO_x作为催化剂, 用

于甘油气相脱水反应. X-射线衍射(XRD)、热重-差热法(TG-DTG)、氨程序升温脱附(NH₃-TPD)、红外光谱(FT-IR)和紫外漫反射可见光谱(DR UV-vis)等表征, 探讨了酸改性和负载WO_x的蒙脱石对催化剂催化性能的影响.

蒙脱石经过20wt%的硫酸、盐酸、磷酸和乙酸的活化, 酸性增加. 四种酸改性的蒙脱石对甘油气相脱水反应均有催化活性, 这是因为在蒙脱石活化过程中, H⁺经过阳离子交换反应进入蒙脱石层间, 同时蒙脱石八面体中的部分Al³⁺被浸出, 使层板上出现不饱和Al³⁺, 为催化剂提供了L酸位, 蒙脱石硅氧四面体上的Si-OH以及[AlO₄]上吸附的H₃O⁺提供了B酸位.

XRD分析表明, 负载WO_x的蒙脱石表面存在WO_{2.72}, WO_{2.9}和WO₃三种不同类型的WO_x, 当钨负载量从12 wt%增至16 wt%, 孤立的单斜晶系WO₃晶粒增多. NH₃-TPD和DR UV-vis结果表明, WO_x负载在蒙脱石表面以[WO₅/WO₆](B酸位)、[WO₄]和单斜晶系WO₃相(L酸位)形式存在. 蒙脱石上负载WO_x能够调节催化剂的酸强度、酸量和酸位. 随着钨负载量从4 wt%增至12 wt%, 丙烯醛收率从40.9%增加到67.3%; 进一步增加钨负载量到16 wt%, 丙烯醛收率降为50.7%. 结果发现, 随着钨负载量的增加, 催化活性组分含量增加, [WO₅/WO₆](B酸位)增加, 使催化活性增加; 当W负载量达到16 wt%时, WO_x分散性降低, 且在催化剂表面形成孤立的单斜晶系WO₃相(L酸位), 不利于提高丙烯醛选择性. 当反应温度为320 °C, 甘油水溶液浓度为15 wt%时, 磷酸活化蒙脱石负载12 wt%W的催化剂上甘油转化率为89.6%, 丙烯醛收率达到73.3%.

关键词: 甘油; 丙烯醛; 脱水; WO_x; 酸活化粘土; 催化剂

收稿日期: 2017-01-13. 接受日期: 2017-03-10. 出版日期: 2017-06-05.

*通讯联系人. 电话/传真: (0571)88320062; 电子信箱: clay@zjut.edu.cn

基金来源: 国家自然科学基金(21373185, 41672033, 21506188, 21404090); 浙江省非金属矿工程研究中心开放基金项目(ZD2015K07); 绿色化学合成技术国家重点实验室培育基地开放基金项目(GCTKF2014006); 浙江省竹子高效加工重点实验室开放基金项目(2016); 北京化工大学化工资源有效利用国家重点实验室开放基金项目(CRE-2016-C-303).

本文的英文电子版由Elsevier出版社在ScienceDirect上出版(<http://www.sciencedirect.com/science/journal/18722067>).